REGULAR ARTICLE

How accurate are electronic structure methods for actinoid chemistry?

**Boris B. Averkiev · Manjeera Mantina ·
Rosendo Valero · Ivan Infante · Attila Kovacs ·
Donald G. Truhlar · Laura Gagliardi**

Abstract The CASPT2, CCSD, and CCSD(T) levels of
wave function theory and seven density functionals were
tested against experiment for predicting the ionization
potentials and bond dissociation energies of actinoid
monoxides and dioxides with their cations. The goal is to
guide future work by enabling the choice of an appropriate
method when performing calculations on actinoid-con-
taining systems. We found that four density functionals,
namely MPW3LYP, B3LYP, M05, and M06, and three
levels of wave function theory, namely CASPT2, CCSD,
and CCSD(T), give similar mean unsigned errors for acti-
noid–oxygen bond energies and for ionization potentials of
actinoid oxides and their cations.

Keywords Actinoids · Electronic structure · Density
functional theory · CASSCF · CASPT2

Dedicated to Professor Pekka Pyykkö on the occasion of his 70th
birthday and published as part of the Pyykkö Festschrift Issue.

B. B. Averkiev · M. Mantina · R. Valero ·
D. G. Truhlar · L. Gagliardi (✉)
Department of Chemistry and Supercomputing Institute,
University of Minnesota, 207 Pleasant St. SE, Minneapolis,
MN 55455-0431, USA
e-mail: gagliard@umn.edu

D. G. Truhlar
e-mail: truhlar@umn.edu

I. Infante
Kimika Fakultatea, Euskal Herriko Unibertsitatea
and Donostia International Physics Center (DIPC),
P.K. 1072, 20080 Donostia, Euskadi, Spain

A. Kovacs
European Commission, Joint Research Centre,
Institute for Transuranium Elements,
P.O. Box 2340, 76125 Karlsruhe, Germany

A. Kovacs
Research Group for Materials Structure and Modeling
of the Hungarian Academy of Sciences,
Budapest University of Technology and Economics,
Szt. Gellért tér 4, 1111 Budapest, Hungary

1 Introduction

Actinoid chemistry is important for reactor waste man-
agement [1–3], and actinoids serve as catalysts for a variety
of reactions [4–7], but understanding actinoid chemistry
poses formidable challenges to both experimental and
computational chemists. From a computational point of
view, in order to be able to treat actinoid chemistry, we
need electronic structure methods capable of properly
describing both electron correlation and relativistic effects
in systems that often have large multireference character.

Many electronic structure studies have appeared in the
literature, involving both wave function theory (WFT) and
density functional theory (DFT). The complete active space
(CAS) self-consistent field (SCF) method [8] followed by
multireference second-order perturbation theory (CASPT2)
[9] and DFT with the original B3LYP [10–13] density
functional (which is based on the VWN3 approximation for
the local spin density component) were tested against
experiment for the prediction of bond distances and
vibrational frequencies in uranium triatomic molecules and
cations [14, 15]. Successively, the CASPT2 [9], relativistic
coupled cluster calculations with single and double exci-
tations (CCSD) [17, 18], and relativistic coupled cluster
calculations with single and double excitations and

Springer

quasiperturbative treatment of connected triple excitations (CCSD(T)) [19, 20] levels of WFT were tested against experiment for ionization potentials of actinoid monoxides and dioxides [16]. In the current paper, we present tests for a larger set of experimental bond dissociation energies in which we include actinoid dioxides and their cations and dications, and, in addition, we test newer density functionals. In particular, the MPW3LYP [21], MOHLYP [22], M05 [23], M06-L [24], and M06 [25] density functionals are tested against both some of the previous [14, 16] data and all of the new test sets. We also checked the performance of an additional older functional, namely the PW91 [26] functional, for these systems, because it was shown [27] that it performs well for vibrational frequencies of the triatomic molecules NUN, NUO$^+$, and CUO. In related work, Austin et al. [28] tested the B3LYP, M05, M06-L, and M06 density functionals and two others against experiment and compared them with CCSD(T) and CAS-PT2 results for actinoid reaction energies; they found that "the M06 functional definitely stands out as being more successful than the other five functionals tested" and "is competitive with high-level ab initio methods" for these reaction energies. The present tests should be particularly useful in that all density functionals and WFT methods mentioned so far are compared to the same sets of data, allowing a consistent comparison.

2 Methods

In the following, we will describe the details of the WFT-based calculations followed by the details of the DFT calculations.

2.1 WFT calculations of bond dissociation energies

Calculations were performed using CASSCF and CASPT2. Scalar relativistic effects were included using the Douglas-Kroll-Hess Hamiltonian to second order [29, 30]. For these calculations, we used a relativistic ANO-RCC basis set of triple zeta quality [31, 32], as implemented in the MOL-CAS 7.4 package [33].

For actinoid monoxides AnO (where An denotes an actinoid, in particular, Th, Pa, U, Np, Pu, Am, or Cm), a full valence active space includes 17 orbitals, in particular 13 from the actinoid and four from the oxygen. In the CASSCF calculations, we used an active space of 16 orbitals obtained by omitting the 2s orbitals of oxygen. For monoxides, the largest number of electrons in these active space orbitals is 14 for CmO. In the subsequent CASPT2 calculations, the orbitals up to the 5d of the actinoid and the 1s of oxygen were kept frozen, while the remaining valence and semi-valence orbitals, now including the

6s and 6p of the actinoid and the 2s of oxygen, were correlated. The full valence active space of actinoid dioxides AnO$_2$ contains 21 orbitals, but calculations with a complete active space this large are not feasible, so the 2s orbitals of oxygen, the two lowest $6d\pi_g$ bonding orbitals, the corresponding antibonding orbitals, and one σ_g^* antibonding orbital are treated as inactive. Thus, the active space is composed of 14 orbitals, occupied primarily by the 5f, 6d, and 7s orbitals of the actinoid atom and the 2p orbitals of the oxygen atoms. By applying the same truncation along the whole series, the largest active space in all our calculations contains 14 electrons in 14 orbitals for CmO$_2$.

Spin–orbit coupling was included using the complete-active-space state-interaction method, CASSI [34, 35], which employs an effective one-electron spin–orbit (SO) Hamiltonian, based on a mean field approximation to the two-electron contribution [36]. Note that a CASSI calculation, like a CASSCF calculation, does not include dynamical correlation. To include this, the spin-free CASPT2 energies are used as diagonal matrix elements in the CASSI treatment; this is called spin–orbit-corrected CASPT2 (SO-CASPT2).

To assist in judging the validity of the CASPT2 results, we performed exact 2-component (X2C) [37, 38] relativistic calculations at the CCSD and CCSD(T) levels using the DIRAC08 program [39]. Note that X2C is also called infinite-order two-component (IO2C). In these coupled cluster calculations, we correlated the electrons in the 6s, 6p, 5f, 6d, and 7s orbitals of the actinoid atom and the four valence electrons of the 2p orbitals of the oxygen. We then restricted the set of virtual orbitals to those most important for valence and sub-valence correlation by deleting virtual orbitals with an orbital energy above 10 E$_h$.

Note that Dyall's transformation [38] allows one to separate a four-component relativistic treatment into spin-free and spin–orbit contributions. The X2C transformation [37] to a two-component treatment that is used here is based only on the spin-free part, i.e., we use the Dirac-Coulomb operator without the Breit spin–orbit term. Therefore, we add the spin–orbit contribution to the close coupling calculations as the difference between the SO-CASPT2 result and the spin-free CASPT2 result.

For the CCSD and CCSD(T) calculations, we used an uncontracted double-zeta 26s23p17d13f2g basis set [40] for actinoid atoms and the cc-pVTZ basis set [41] for oxygen atoms.

The geometries for all WFT calculations are SO-CASPT2 geometries. (Please note that the statement in [16] that some geometries are spin-free CASPT2 is a typo.) The zero-point vibrational energy (ZPE) change for the WFT calculations was taken to be the same as in the M06 calculations (calculated from scaled M06 frequencies as described in Sect. 2.3).

2.2 WFT calculations of ionization potentials

The WFT calculations of ionization potentials (IPs) are updated in two respects from those published [16] previously. Previously, PuO_2, PuO_2^+, and PuO_2^{2+} were computed by RASPT2 [42, 43]; in the present article, all PT2 results are CAS, not RAS. Previously, the change in ZPE was limited to the symmetric stretching mode; here, a full ZPE correction is made, based on DFT, as mentioned at the end of Sect 2.1.

2.3 DFT calculations

For ionization potentials and bond dissociation energies of actinoid monoxides and dioxides, DFT calculations were performed with the relativistic MWB60 small-core effective core potential [44] and the Stuttgart/Dresden-segmented ECP60MWB_SEG basis set [45] for actinoids and the 6-311+G(2df) basis set [46] for oxygen atoms. All calculations were carried out with *Gaussian09* [47].

Geometries for these calculations were optimized by DFT for each functional tested. (For additional comparisons, we also carried out single-point energy calculations at SO-CASPT2 geometries, but these results are given only in supporting information). For all DFT calculations, we used an integration grid that has 400 radial shells and 974 angular points per shell. All DFT calculations were performed without enforcing symmetry on the orbitals. All calculations are spin unrestricted, although for some of the singlets, the optimized wave functions retain doubly occupied orbitals as in the restricted theory even when we started with a guess that destroys spin symmetry.

Harmonic ZPEs were scaled using the following scale factors: M05, 0.977; M06, 0.981; M06-L, 0.978; B3LYP, 0.983; MOHLYP, 1.022; MPW3LYP, 0.983, and PW91, 1.007 [48, 49].

We added the spin–orbit contribution to all DFT calculations as the difference between the SO-CASPT2 result and the spin-free CASPT2 result (although readers who are interested in the results without such additions may find them in the supporting information).

3 Results

All numerical results in the article proper include spin–orbit and ZPE contributions, and all DFT results in the article proper are at DFT geometries. For the specialist, the supporting information gives results without spin–orbit, without ZPE, and without both. The supporting information also gives DFT results at spin-free CASPT2 geometries.

Tables 1, 2, 3, and 4 report the first and second ionization potentials (IPs) of AnO and AnO_2 obtained with WFT and DFT, and Tables 5 and 6 give bond dissociation energies for breaking An–O bonds. Because the values in Tables 1, 2, 3, 4, 5, and 6 include ZPEs, they are enthalpy changes at 0 K.

In tables, MUE(7) means the mean unsigned error for the seven previous rows. MUE(x) in the last row of a table means the mean unsigned for all x rows of data in the table. By error, we mean the deviation from experiment. In this regard, the reader should be aware that most of the experimental data have an error bar large enough that it must be taken into account in drawing conclusions about the comparison of theory to experiment; we cannot state that a method is better than another when their difference is within the experimental error bar. We will therefore concentrate our attention mainly on analyzing which theoretical models predict results that agree with experiment within the error bars.

4 Discussion

In discussing numerical results, we will discuss only those including spin–orbit and ZPE contributions, and we will discuss DFT results only for calculations at DFT

Table 1 First and Second Ionization Potentials (in eV) of AnO by WFT

	CASPT2	CCSD	CCSD(T)	Exp[a]
ThO	6.56	6.39	6.53	6.6035 ± 0.0008
PaO	6.28	6.18	6.31	5.9 ± 0.2
UO	6.05	5.92	5.99	6.0313 ± 0.0006
NpO	5.97	5.97	6.04	6.1 ± 0.2
PuO	6.17	5.95	6.00	6.1 ± 0.2
AmO	6.22	6.02	6.04	6.2 ± 0.2
CmO	6.68	6.42	6.46	6.4 ± 0.2
MUE(7)	0.13	0.15	0.13	0.14[b]
ThO+	11.94	11.92	11.99	11.8 ± 0.7
PaO+	12.10	12.36	12.46	11.8 ± 0.7
UO+	13.08	12.41	12.39	12.4 ± 0.6
NpO+	13.44	13.28	13.23	14.0 ± 0.6
PuO+	14.36	14.11	14.00	14.0 ± 0.6
AmO+	15.04	15.83	15.71	14.0 ± 0.6
CmO+	15.88	15.08	15.08	15.8 ± 0.4
MUE(7)	0.45	0.58	0.58	0.63[b]
MUE(14)	0.29	0.37	0.36	0.39[b]

[a] Most of the experimental values were obtained through indirect measurements [57]; Values for ThO and UO were accurately measured by Heaven and co-workers using REMPI method [50, 51]

[b] The MUE(x) for the experiment is referred to the average error bar

Table 2 First and second ionization potentials (eV) of AnO from DFT Calculations

	M05	M06	M06-L	B3LYP	MOHLYP	MPW3LYP	PW91	Exp[a]
ThO	6.61	6.84	6.45	6.52	6.17	6.57	6.47	6.6035 ± 0.0008
PaO	6.31	6.67	5.31	6.30	5.78	6.32	8.40	5.9 ± 0.2
UO	5.71	6.09	5.55	6.18	5.84	6.21	6.22	6.0313 ± 0.0006
NpO	5.63	5.79	5.42	6.26	5.85	6.29	6.28	6.1 ± 0.2
PuO	5.75	5.88	5.54	6.38	5.97	6.42	6.39	6.1 ± 0.2
AmO	6.04	6.08	5.77	6.50	6.21	6.54	6.59	6.2 ± 0.2
CmO	6.14	6.27	5.87	6.67	6.19	6.71	6.63	6.4 ± 0.2
MUE(7)	0.28	0.26	0.49	0.23	0.19	0.25	0.56	0.14[b]
ThO[+]	11.63	11.84	11.36	12.21	11.82	12.24	12.18	11.8 ± 0.7
PaO[+]	12.36	12.42	12.86	12.63	14.81	12.67	12.69	11.8 ± 0.7
UO[+]	13.01	12.95	12.75	13.08	12.63	13.11	13.01	12.4 ± 0.6
NpO[+]	13.54	13.60	13.29	13.75	13.14	13.78	13.56	14.0 ± 0.6
PuO[+]	14.19	14.38	14.05	14.42	13.80	14.44	14.22	14.0 ± 0.6
AmO[+]	15.29	15.37	14.93	15.33	14.69	15.36	15.12	14.0 ± 0.6
CmO[+]	15.28	15.40	15.15	15.44	15.11	15.47	15.49	15.8 ± 0.4
MUE(7)	0.54	0.54	0.60	0.61	0.81	0.63	0.57	0.63[b]
MUE(14)	0.41	0.40	0.54	0.42	0.50	0.44	0.56	0.39[b]

[a] Most of the experimental values were obtained through indirect measurements [57]; Values for ThO and UO were accurately measured by Heaven and co-workers using REMPI method [50, 51]

[b] The MUE(x) for the experiment is referred to the average error bar

Table 3 First and second ionization potentials (in eV) of AnO$_2$ from WFT calculations

	CASPT2	CCSD	CCSD(T)	Exp[a]
ThO$_2$	8.49	8.58	8.58	8.9 ± 0.4
PaO$_2$	5.71	5.93	6.04	5.9 ± 0.2
UO$_2$	6.24	6.05	6.07	6.128 ± 0.003
NpO$_2$	6.30	5.91	6.01	6.33 ± 0.18
PuO$_2$	6.23	5.62	5.73	7.03 ± 0.12
AmO$_2$	6.80	6.66	6.55	7.23 ± 0.15
CmO$_2$	8.31	7.77	7.60	8.5 ± 1.0
MUE(7)	0.31	0.51	0.53	0.29[b]
ThO$_2^+$	15.09	15.86	15.39	16.6 ± 1.0
PaO$_2^+$	16.98	16.93	16.87	16.6 ± 0.4
UO$_2^+$	14.38	14.13	14.01	14.6 ± 0.4
NpO$_2^+$	15.59	15.44	15.26	15.1 ± 0.4
PuO$_2^+$	15.38	15.84	15.62	15.1 ± 0.4
AmO$_2^+$	16.29	16.45	16.33	15.7 ± 0.6
CmO$_2^+$	16.17	16.10	15.95	17.9 ± 1.0
MUE(7)	0.74	0.74	0.76	0.60[b]
MUE(14)	0.53	0.62	0.65	0.45[b]

[a] Most of the experimental values were obtained through indirect measurements [57]; Value for UO$_2$ was accurately determined by Han et al. [52] using REMPI method

[b] The MUE(x) for the experiment is referred to the average error bar

geometries. Before discussing the tables, though, we will briefly discuss the characteristics of the ground states and the Kohn–Sham determinants.

4.1 Ground states and Kohn–Sham determinants

The ground states and dominant electron configurations in the CASSCF calculations for the molecules in Tables 1, 2, 3, 4, 5, and 6 are summarized in [16] and that information will not be repeated here. For the CCSD and CCSD(T) calculations, we have converged the Hartree–Fock single-configuration reference wave functions to the dominant determinant identified by the CASSCF calculations.

For the DFT calculations on the molecules in Tables 1, 2, 3, 4, 5, and 6, in every case, we checked all possible values of the spin projection quantum number M_S to find the lowest-energy spin state and orbital composition. We compared our findings for the lowest-energy spin state in DFT to the lowest spin state in spin-free CASPT2, as given in [16]. We found that it agreed in every case except for M05, M06, M06-L, and MOHLYP calculations of neutral UO, for which it turned out that a triplet state is lower than the quintet state that is predicted to be the ground state by WFT calculations.

Spin contamination is not severe (see Table S35 of Supporting Information for a detailed table). For example, consider the dioxides. For neutral AnO$_2$, the expectation value of S^2 is within 1% of $M_S (M_S + 1)$ in all cases, where M_S, as usual, denotes the projection quantum number of electron spin. The AnO$_2^+$ monocations satisfy this condition within 1% for $M_S \leq 3/2$ and within 2% for other MS.

Table 4 First and second ionization potentials (eV) of AnO_2 from DFT calculations

	M05	M06	M06-L	B3LYP	MOHLYP	MPW3LYP	PW91	Exp[a]
ThO_2	8.31	8.52	8.00	8.56	8.02	8.62	8.39	8.9 ± 0.4
PaO_2	5.82	6.13	6.59	6.34	7.15	6.35	6.27	5.9 ± 0.2
UO_2	6.08	6.07	5.81	6.25	5.89	6.29	6.27	6.128 ± 0.003
NpO_2	6.31	6.21	5.77	6.36	6.08	6.36	6.40	6.33 ± 0.18
PuO_2	6.46	6.60	6.17	6.61	6.29	6.61	6.58	7.03 ± 0.12
AmO_2	6.98	6.96	6.58	7.17	6.22	7.17	6.84	7.23 ± 0.15
CmO_2	8.21	8.22	7.74	8.27	7.46	8.29	7.82	8.5 ± 1.0
MUE(7)	0.27	0.25	0.67	0.24	0.77	0.23	0.38	0.29[b]
ThO_2^+	16.34	16.43	16.07	16.30	15.94	16.32	16.38	16.6 ± 1.0
PaO_2^+	16.70	17.03	16.44	16.93	17.47	17.00	16.70	16.6 ± 0.4
UO_2^+	15.35	15.14	14.86	15.08	14.49	15.09	14.96	14.6 ± 0.4
NpO_2^+	16.30	16.27	16.02	16.21	15.45	16.23	15.94	15.1 ± 0.4
PuO_2^+	16.45	16.40	15.94	16.32	15.72	16.34	16.13	15.1 ± 0.4
AmO_2^+	16.50	16.59	16.18	16.44	15.90	16.45	16.25	15.7 ± 0.6
CmO_2^+	16.41	16.48	16.00	16.52	15.60	16.53	16.04	17.9 ± 1.0
MUE(7)	0.85	0.84	0.73	0.80	0.73	0.81	0.71	0.60[b]
MUE(14)	0.56	0.55	0.70	0.52	0.75	0.52	0.54	0.45[b]

[a] Most of the experimental values were obtained through indirect measurements [57]; Value for UO_2 was accurately determined by Han et al. [52] using REMPI method

[b] The MUE(x) for the experiment is referred to the average error bar

For the AnO_2^{2+} dications, the condition is satisfied within 1% for $M_S \leq \frac{1}{2}$, within 2% for $M_S = 1$, within 4% for $M_S = 3/2$, and within 6% for $M_S = 2$. The only exception is singlet ThO_2^{2+} molecule, for which S^2 has high values (0.52–0.70) except for the MOHLYP functional ($S^2 = 0.09$). For the B3LYP functional, the optimization of the ThO_2^{2+} as closed-shell singlet (i.e. with constrained $S^2 = 0.0$) results in Th–O distance 1.851 Å, while the optimization as an open-shell singlet with $S^2 = 0.7$ results in Th–O distance 1.909 Å. The latter structure is 7.6 kcal/mol lower than the former one. For analogous M06 calculations of ThO_2^{2+} the distance of closed-shell singlet is 1.800 Å, for open-shell singlet is 1.867 Å. The latter structure is 2.2 kcal/mol lower than the former one.

Comparing the orbital character of the DFT determinants to the orbital composition of the CASSCF wave function is harder because in most cases where the contribution of the Hartree–Fock determinant in the CASSCF wave function is less than 80% (see Tables 3 and 4 of [16]), the Kohn–Sham orbitals break symmetry. In several cases, even when the system can be described to better than 90% by a single configuration, two singly occupied orbitals (for example, the δ and ϕ orbitals in the cases of NpO_2^+ and the isoelectronic PuO_2^{2+}) have very similar orbital energies, and the Kohn–Sham orbitals are mixtures of these orbitals. When the orbitals do not break symmetry, we can compare the DFT orbital character to the dominant orbital composition case of the CASSCF wave function. As an

example, consider the case of M06 calculations for AnO_2 and their cations. In most cases, for M06 method, the DFT orbitals correspond to the CASPT2 orbitals of AnO_2 and their cations. The exceptions are UO_2, NpO_2, and PuO_2 molecules. For NpO_2, M06 predicts a $^4\Phi_u$ ground state when compared with ^4H_g for CASPT2, and for PuO_2, M06 predicts a $^5\Sigma_g$ ground state when compared with $^5\Phi_u$ for CASPT2. For the UO_2 molecule, the M05, M06, and M06-L functionals give the ground state as ^3H_g, while other DFT methods and WFT methods give the $^3\Phi_u$ state as the ground state. The difference is due to the HOMO orbital, which is the 7s orbital of U for the $^3\Phi_u$ state and $5f\delta$ orbital of U for the ^3H_g state. In the latter case, singly occupied δ and ϕ orbitals are mixed, and their linear combinations constitute two broken-symmetry orbitals with the same energy.

4.2 Ionization potentials

When comparing WFT results with DFT results, we have to contextualize the values with respect to available experimental data. The most accurate experiments are for ThO [50], UO [51], and UO_2 [52], where the error on the IP is less than or equal to 0.003 eV. CASPT2 and CCSD(T) perform rather well for these cases, with an MUE(3) of 0.06 eV (where MUE(x) denotes mean unsigned error averaged over x molecules), while CCSD performs worse—the MUE(3) is 0.13 eV. CASPT2 overcomes this deficiency by a multiconfigurational treatment of static correlation [8, 9], and

Table 5 Bond Energies (in kcal/mol) for AnO_2 AnO_2^+ and AnO_2^{2+} from WFT Calculations

	CASPT2	CCSD	CCSD(T)	Exp.[a]
ThO_2	147	139	144	164 ± 3
PaO_2	190	172	181	187 ± 11
UO_2	146	170	183	180 ± 3
NpO_2	169	143	158	152 ± 10
PuO_2	134	128	144	144 ± 5
AmO_2	119	96	110	122 ± 16
CmO_2	108	81	95	97 ± 17
MUE(7)	14	17	7	9[b]
ThO_2^+	103	88	96	111 ± 9
PaO_2^+	203	177	185	187 ± 7
UO_2^+	181	171	182	178 ± 3
NpO_2^+	162	144	156	146 ± 5
PuO_2^+	131	130	143	122 ± 9
AmO_2^+	117	84	98	98 ± 13
CmO_2^+	73	51	88	49 ± 14
MUE(7)	13	9	13	9[b]
ThO_2^{2+}	30	−4	16	0 ± 41
PaO_2^{2+}	92	73	85	76 ± 26
UO_2^{2+}	143	127	140	127 ± 7
NpO_2^{2+}	113	94	109	121 ± 2
PuO_2^{2+}	104	92	107	97 ± 23
AmO_2^{2+}	67	67	83	61 ± 31
CmO_2^{2+}	41	28	47	0 ± 36
MUE(7)	18	10	19	24
MUE(21)	15	12	13	14

[a] The experimental values from Marçalo and Gibson work [57] obtained using Born cycle utilizing the measured ionization potentials
[b] The MUE(x) for the experiment is referred to the average error bar

density functional theory includes some static correlation in the exchange potential [53–56]. On the same molecules, the M05, M06, MPW3LYP, and B3LYP functionals give MUE(3) = 0.12 eV, PW91 gives 0.16 eV, MOHLYP gives 0.29 eV, and M06-L gives 0.32 eV.

For the other set of AnO molecules, there is no direct measurement of the IP, and the experimental error bar of the first ionization potential is rather large, about 0.2 eV [57]. Inspection of Table 1 shows that the mean unsigned error (MUE) for CASPT2, CCSD, and CCSD(T) for the first IP of AnO is, respectively, 0.13, 0.15, and 0.13 eV. Thus, among the wave function methods, all three perform within the experimental uncertainty. The DFT results for IPs are reported in Table 2. For first IPs, the MUE is 0.28, 0.26, 0.49, 0.23, 0.19, 0.25, and 0.56 eV for M05, M06, M06-L, B3LYP, MOHLYP, MPW3LYP, and PW91, respectively.

For the second IP, the experiments show even larger error bars, ranging from 0.4 eV for CmO+ to 0.6–0.7 eV

for the remaining AnO monocationic species [57]. Almost all WFT and DFT methods agree with experiment within these limits (the only exception being MOHLYP), in particular the WFT methods give MUE values of 0.45 (CASPT2), 0.58 (CCSD), and 0.58 eV (CCSD(T)). The MUEs are 0.54, 0.54, and 0.60 eV for M05, M06, M06-L, respectively, and 0.61, 0.81, 0.63, and 0.57 eV for B3LYP, MOHLYP, MPW3LYP, and PW91, respectively.

Now we consider the AnO_2 systems. The IPs of these molecules have been measured with three different methods, each of them bearing a different error bar. The only very accurate direct measurement (using the REMPI method) has been carried out for UO_2 [52]. The second type of experiment employed to measure the first ionization potential of some of the actinoid species is a well-established electron-transfer bracketing technique, which is an indirect approach that carries an error in the range of 0.1–0.2 eV. In particular, this method has been employed by Marçalo and Gibson [57] to obtain the IPs of NpO_2, PuO_2, and AmO_2, with error bars of 0.18, 0.12, and 0.15 eV, respectively. Table 4 shows that WFT methods tend to give results lower than experiment by more than the experimental error bar, more prominently for the CCSD approaches. This has been discussed previously [16], in particular for the PuO_2 molecule, where the first IP was computed to be considerably lower than the experiment. The first IP of PuO_2 is computed by DFT to range from a minimum of 6.17 eV for M06-L to a maximum of 6.61 eV for MPW3LYP and B3LYP. We notice that these values still fall far from the experimental error bar, and quantum chemical methods therefore suggest that the actual value of the first IP of PuO_2 is closer to 6–6.5 eV than to 7 eV.

CASPT2 and five of the density functionals give very similar values for the IP of NpO_2, all in a small window of energies, between 6.21 and 6.36 eV. The 6.21–6.36 eV window agrees well with the experiment. The CCSD, CCSD(T), MOHLYP, and M06-L calculations give a lower IP, outside the experimental error bar.

For AmO_2, we encounter a similar situation to PuO_2, with all computed first ionization potentials below the experimental error bar; however, they are closer to experiment than in the case of PuO_2. WFT shows the largest differences, while B3LYP and MPW3LYP give IPs inside the experimental error bar. Further experimental work to confirm that the actual ionization potentials are lower than the one measured will be difficult due to the hazardous nature of the materials, and the bracketing technique will probably remain the most reliable experimental method for some time.

The third method used to measure the IP of actinoid species is an indirect method based on the reactions of actinoid molecules with species of known IPs [57]. In this case, the error bars are quite large, 0.2 eV for PaO_2,

Table 6 Bond Energies (kcal/mol) for AnO_2, AnO_2^+, and AnO_2^{2+} from DFT Calculations

	M05	M06	M06-L	B3LYP	MOHLYP	MPW3LYP	PW91	Exp.[a]
ThO_2	159	155	166	157	163	158	176	164 ± 3
PaO_2	165	169	199	179	186	181	146	187 ± 11
UO_2	172	170	179	171	182	172	193	180 ± 3
NpO_2	163	167	172	154	168	155	178	152 ± 10
PuO_2	148	153	159	141	155	142	165	144 ± 5
AmO_2	109	115	122	108	112	109	128	122 ± 16
CmO_2	104	106	116	101	114	102	125	97 ± 17
MUE(7)	10	11	10	7	8	6	21	9[b]
ThO_2^+	121	116	130	111	121	112	132	111 ± 9
PaO_2^+	176	181	169	178	154	179	195	187 ± 7
UO_2^+	163	171	173	169	180	170	191	178 ± 3
NpO_2^+	146	156	163	150	161	151	173	146 ± 5
PuO_2^+	126	131	139	130	141	131	154	122 ± 9
AmO_2^+	88	95	104	93	112	94	123	98 ± 13
CmO_2^+	58	62	74	65	86	67	98	49 ± 14
MUE(7)	8	8	15	7	18	7	25	9[b]
ThO_2^{2+}	12	11	22	17	25	18	35	0 ± 41
PaO_2^{2+}	72	76	88	79	94	81	103	76 ± 26
UO_2^{2+}	102	115	119	118	132	119	141	127 ± 7
NpO_2^{2+}	84	94	100	93	107	94	117	121 ± 2
PuO_2^{2+}	81	87	98	88	99	90	112	97 ± 23
AmO_2^{2+}	61	67	74	67	83	69	97	61 ± 31
CmO_2^{2+}	28	34	51	37	71	39	82	0 ± 36
MUE(7)	18	14	18	16	23	16	30	24[b]
MUE(21)	12	11	14	10	16	10	25	14[b]

[a] The experimental values from Marçalo and Gibson work [57] obtained using Born cycle utilizing the measured ionization potentials

[b] The MUE(x) for the experiment is referred to the average error bar

increasing to 0.4 for ThO_2 and to 1.0 eV for CmO_2. For these cases, WFT calculations yield values falling within the experimental limits. For PaO_2, M05 and M06 methods give values falling within the experimental limits, while other DFT functionals overestimate the experimental value of 5.9 eV, especially MOHLYP (7.15 eV). For ThO_2, M06, B3LYP, and MPW3LYP give values falling within the experimental limits, while other functionals underestimate the experimental value 8.9 eV.

For the second IPs, the experimental error bars are rather large, ranging from 0.4 to 1.0 eV [57]. As in the case of the monoxides, the calculations show significant discrepancies from the middle experimental value. On average, WFT and DFT have roughly the same MUE(7); however, in specific cases, they may differ from each other by a significant amount. For example, looking at the second IP of UO_2, the CASPT2 calculation gives 14.38 eV, CCSD(T) gives 14.01 eV, and M05, which has performed well in cases discussed above, yields a value 1 eV higher, 15.35 eV. Such discrepancies occur quite often in Tables 3 and 4. Unfortunately, due to the large error bars, the experimental values do not help much in deciding which method is most reliable.

The overall performance of methods for the first and second ionization potentials of AnO and AnO_2 is summarized by MUE(AIP28) in Table 7 (The other rows of this table are discussed below).

4.3 Bond energies

We now consider the performance of the various methods for bond dissociation energies (BDEs), bearing in mind that their experimental values are much more uncertain than those for ionization potentials. This is due to the fact that the BDEs are computed by a Born cycle using the measured ionization potentials [57], hence inheriting their errors along with the errors for other steps in the cycle. Furthermore, we must consider the following issue regarding the CASPT2 calculations. When calculating the reaction $AnO_2 \rightarrow AnO + O$, it is difficult to keep a balanced active space between the AnO_2 and its dissociation products because a full valence

Table 7 Performance of Tested Methods for 28 Actinoid Ionization Potentials MUE(AIP28) for 21 Actinoid Bond Dissociation Energies MUE(ABDE21) and for the Actinoid Composite Energy Database of all 49 Ionization Potential and Bond Dissociation Energy Data MUE(ACE49)

	CASPT2	CCSD	CCSD(T)	M05	M06	M06-L	B3LYP	MOHLYP	MPW3LYP	PW91
In kcal/mol										
MUE(ABDE21)	15	12	13	12	11	14	10	16	10	25
In eV										
MUE(AIP28)	0.41	0.50	0.50	0.49	0.47	0.62	0.47	0.63	0.48	0.55
MUE(ABDE21)	0.65	0.53	0.56	0.52	0.47	0.63	0.43	0.71	0.43	1.10
MUE(AC49)	0.51	0.51	0.52	0.50	0.47	0.63	0.45	0.66	0.46	0.79

active space is impractical for AnO_2, and we need to truncate the space (see Sect. 2). This lack of balance at the CASSCF level could be reflected in the description of the correlation energy, and the error at the CASPT2 level can be larger than what is expected on the basis of calculations where a full valence active space is employed. Inspection of Table 5 confirms this by showing that the MUE for CASPT2 is slightly larger than that for CCSD(T), especially for the dissociation of the neutral AnO_2 (14 vs. 7 kcal/mol).

DFT methods perform well, especially B3LYP and MPW3LYP. The M06 functional shows slightly larger differences from the experiment, but still performs well.

The overall performance of methods for dissociation energies of AnO_2 is shown by MUE(ABDE21) in Table 7. The bad performance of PW91 is related to systematic overestimation of the dissociation energies of AnO_2 by this method, with the exception of PaO_2, for which PW91 underestimates the bond dissociation energy by 41 kcal/mol.

4.4 Bond distances

The Ac–O bond distance was optimized for all oxides with the various density functionals. In Fig. 1, we report the deviations of DFT bond distances from the CASPT2 bond distances (Å). The absolute values are reported in Supporting Information. The chart shows a nearly systematic

deviation of bond distances predicted by the various exchange–correlation functionals from those predicted by CASPT2.

4.5 Overall assessment

The overall performance for both ionization potentials and bond dissociation energies is given by MUE(AC49) in Table 7. Four of the density functionals (those containing a nonzero fraction of Hartree–Fock exchange) and all three WFT methods show very similar average performance. Among the three functionals without Hartree–Fock exchange, the M06-L and MOHLYP functionals perform better than PW91.

5 Conclusions and outlook

The systems discussed in this paper pose non-trivial challenges because of their complex electronic structure and relativistic effects. We have compared the performance of different methods with the hope of making future users more aware of their strengths and limitations.

The CASPT2 wave function method used here has been used successfully in studying many actinoid-containing systems [58–63]. Recent developments of the Cholesky decomposition (CD) approach (they have not been employed in the present study), in combination with the

Fig. 1 Deviations of DFT bond distances from the CASPT2 bond distances (Å)
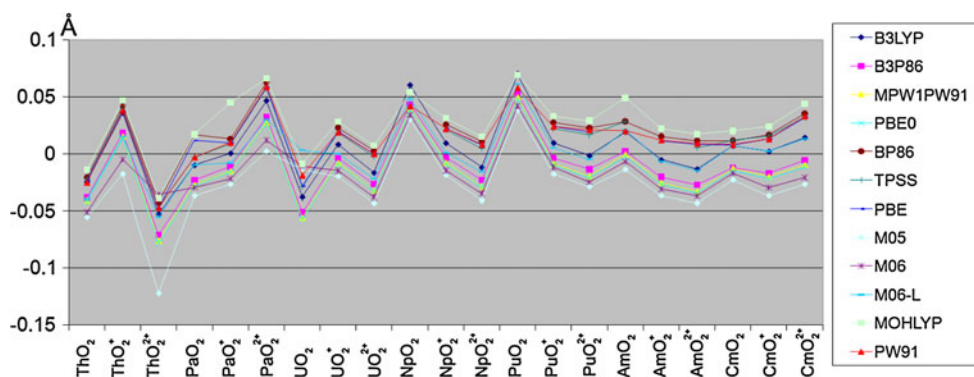
CASPT2 method [64], have extended the applicability of the CASPT2 method to larger molecular systems. A CD-CASPT2 calculation with 1000 basis functions is nowadays affordable [65]. In addition, CD-CASPT2 calculations can be performed at even lower computational costs and on large systems by invoking the frozen natural orbital (FNO) approximation [66, 67] to effectively reduce the size of the virtual orbital space with no loss of accuracy. However, increasing the molecular size is not sufficient. There are many quantum-chemical problems whose accurate solution is out of reach for CASPT2 because the adequate number of MOs cannot be included in the active space [42]. Wave function methods such as CCSD and CCSD(T) are even more expensive for large systems. Density functional theory on the other hand remains quite affordable for large systems, and it has had many successes for transition metal chemistry [56, 68]. Here, we find that DFT, at least with well-chosen functionals such as MPW3LYP, B3LYP, M06, and M05, is, on average, as accurate as or more accurate than CASPT2, CCSD, and CCSD(T) methods for bond energies to actinides. These four functionals also provide comparable accuracy for ionization potentials of actinoid compounds.

References

1. Hanschke JM, Stakebake JL (2006) In: Morss LR, Edelstein NM, Fuger NM, Katz JJ (eds) The chemistry of the actinide and transactinide elements, vol 5. Springer, Dordrecht
2. Choppin GR, Jensen MP (2006) In: Morss LR, Edelstein NM, Fuger NM, Katz JJ (eds) Chemistry of the actinides and transactinide elements. Springer, Dordrecht
3. Choppin GR (2007) J Radioanal Nucl Chem 273:695
4. Colmenares CA (1984) Prog Solid State Chem 15:257
5. Barnea E, Eisen MS (2006) Coord Chem Rev 250:855
6. de Almeida KJ, Cesar A (2006) Organometallics 25:3407
7. Stubbert BD, Marks TJ (2007) J Am Chem Soc 129:4253
8. Roos BO, Taylor PR, Siegbahn PEM (1980) Chem Phys 48:157
9. Andersson K, Malmqvist P-Å, Roos BO (1992) J Chem Phys 96:1218
10. Becke AD (1988) Phys Rev A 38:3098
11. Lee C, Yang W, Parr RG (1988) Phys Rev B 37:785
12. Becke AD (1993) J Chem Phys 98:5648
13. Stephens PJ, Devlin FJ, Chabalowski CF, Frisch MJ (1994) J Phys Chem 98:11623
14. Gagliardi L, Roos BO (2000) Chem Phys Lett 331:229
15. Gagliardi L, Heaven MC, Krogh JW, Roos BO (2005) J Am Chem Soc 127:86
16. Infante I, Kovacs A, La Macchia G, Shahi ARM, Gibson JK, Gagliardi L (2010) J Phys Chem A 114:6007
17. Purvis GD, Bartlett RJ (1982) J Chem Phys 76:1910
18. Visscher L, Eliav E, Kaldor U (2001) J Chem Phys 115:9720
19. Raghavachari K, Trucks GW, Pople JA, Head-Gordon M (1989) Chem Phys Lett 157:479
20. Visscher L, Lee TJ, Dyall KG (1996) J Chem Phys 105:8769
21. Zhao Y, Truhlar DG (2004) J Phys Chem A 108:6908
22. Schultz NE, Zhao Y, Truhlar DG (2005) J Phys Chem A 109:11127
23. Zhao Y, Schultz NE, Truhlar DG (2005) J Chem Phys 123:161103
24. Zhao Y, Truhlar DG (2006) J Chem Phys 125:194101
25. Zhao Y, Truhlar DG (2008) Theor Chem Acc 120:215
26. Perdew JP (1991) In: Ziesche P, Eschrig H (eds) Electronic structure of solids '91. Akademie, Berlin
27. Clavaguera-Sarrio C, Ismail N, Marsden CJ, Begue D, Pouchan C (2004) Chem Phys 302:1
28. Austin JP, Burton NA, Hillier IH, Sundararajan M, Vincent MA (2009) Phys Chem Chem Phys 11:1143
29. Douglas N, Kroll NM (1974) Ann Phys 82:89
30. Hess BA (1986) Phys Rev A 33:3742
31. Roos BO, Lindh R, Malmqvist P-Å, Veryazov V, Widmark PO (2005) Chem Phys Lett 409:295
32. Roos BO, Lindh R, Malmqvist P-Å, Veryazov V, Widmark PO, Borin AC (2008) J Phys Chem A 112:11431
33. Aquilante F, De Vico L, Ferre N, Ghigo G, Malmqvist P-Å, Neogrady P, Pedersen TB, Pitonak M, Reiher M, Roos BO, Serrano-Andres L, Urban M, Veryazov V, Lindh R (2010) J Comp Chem 31:224
34. Malmqvist P-Å, Roos BO, Schimmelpfennig B (2002) Chem Phys Lett 357:230
35. Roos BO, Malmqvist P-Å (2004) Phys Chem Chem Phys 6:2919
36. Hess BA, Marian CM, Wahlgren U, Gropen O (1996) Chem Phys Lett 251:365
37. Ilias M, Saue T (2007) J Chem Phys 126:064102
38. Dyall KG (1994) J Chem Phys 100:2118
39. Visscher L, Jensen HJ Aa, Saue T, with new contributions from Bast R, Dubillard S, Dyall KG, Ekström U, Eliav E, Fleig T, Gomes ASP, Helgaker TU, Henriksson J, Iliaš M, Jacob ChR, Knecht S, Norman P, Olsen J, Pernpointner M, Ruud K, Sałek P, Sikkema J (2008) DIRAC, a relativistic ab initio electronic structure program, Release DIRAC08 (see http://dirac.chem.sdu.dk)
40. Dyall KG (2004) Theor Chem Acc 112:403
41. Dunning TH (1989) J Chem Phys 90:1007
42. Malmqvist P-Å, Pierloot K, Shahi ARM, Cramer CJ, Gagliardi L (2008) J Chem Phys 128:204109
43. Rehaman Moughal Shahi A, Cramer CJ, Gagliardi L (2009) Phys Chem Chem Phys 11:10964
44. Kuchle W, Dolg M, Stoll H, Preuss H (1994) J Chem Phys 100:7535
45. Cao XY, Dolg M (2004) J Mol Struct (Theochem) 673:203; (see also the Stuttgart-Cologne basis set site: http://www.theochem.uni-stuttgart.de/pseudopotentials/clickpse.en.html)
46. Krishnan R, Binkley JS, Seeger R, Pople JA (1980) J Chem Phys 72:650
47. Frisch MJ, Trucks GW, Schlegel HB, Scuseria GE, Robb MA, Cheeseman JR, Scalmani G, Barone V, Mennucci B, Petersson GA, Nakatsuji H, Caricato M, Li X, Hratchian HP, Izmaylov AF, Bloino J, Zheng G, Sonnenberg JL, Hada M, Ehara M, Toyota K, Fukuda R, Hasegawa J, Ishida M, Nakajima T, Honda Y, Kitao O, Nakai H, Vreven T, Montgomery JA Jr, Peralta JE, Ogliaro F, Bearpark M, Heyd JJ, Brothers E, Kudin KN, Staroverov VN,

Kobayashi R, Normand J, Raghavachari K, Rendell A, Burant JC, Iyengar SS, Tomasi J, Cossi M, Rega N, Millam NJ, Klene M, Knox JE, Cross JB, Bakken V, Adamo C, Jaramillo J, Gomperts R, Stratmann RE, Yazyev O, Austin AJ, Cammi R, Pomelli C, Ochterski JW, Martin RL, Morokuma K, Zakrzewski VG, Voth GA, Salvador P, Dannenberg JJ, Dapprich S, Daniels AD, Farkas Ö, Foresman JB, Ortiz JV, Cioslowski J, Fox DJ (2009) GAUSSIAN 09 (Revision A.1). Gaussian Inc, Wallingford

48. Alecu IM, Zheng J, Zhao Y, Truhlar DG (2010) J Chem Theory Comput 6:2872
49. Zheng J, Alecu IM, Lynch BJ, Zhao Y, Truhlar DG (2010) Database of frequency scale factors for electronic structure methods. University of Minnesota, Minneapolis. http://comp.chem.umn.edu/freqscale/index.html. Accessed 26 Nov 2010
50. Goncharov V, Heaven MC (2006) J Chem Phys 124:064312
51. Goncharov V, Kaledin LA, Heaven MC (2006) J Chem Phys 125:133202
52. Han JD, Goncharov V, Kaledin LA, Komissarov AV, Heaven MC (2004) J Chem Phys 120:5155
53. Becke AD (2000) J Chem Phys 112:4020
54. Gritsenko OV, Schipper PRT, Baerends EJ (1997) J Chem Phys 107:5007
55. Polo V, Grafenstein J, Kraka E, Cremer D (2003) Theor Chem Acc 109:22
56. Cramer CJ, Truhlar DG (2009) Phys Chem Chem Phys 11:10757
57. Marçalo J, Gibson JK (2009) J Phys Chem A 113:12599
58. Gagliardi L, Pyykkö P, Roos BO (2005) Phys Chem Chem Phys 7:2415
59. Gagliardi L, Pyykkö P (2004) Angew Chem Int Ed 43:1573
60. Gagliardi L (2006) Theor Chem Acc 116:307
61. Gagliardi L, Roos BO (2007) Chem Soc Rev 36:893
62. Infante I, Gagliardi L, Scuseria GE (2008) J Am Chem Soc 130:7459
63. Infante I, Gagliardi L, Wang XF, Andrews L (2009) J Phys Chem A 113:2446
64. Aquilante F, Pedersen TB, Lindh R, Roos BO, De Meras AS, Koch H (2008) J Chem Phys 129:024113
65. Aquilante F, Malmqvist P-Å, Pedersen TB, Ghosh A, Roos BO (2008) J Chem Theory Comput 4:694
66. Aquilante F, Gagliardi L, Pedersen TB, Lindh RJ (2009) Chem Phys 130:154107
67. La Macchia G, Manni GL, Todorova TK, Brynda M, Aquilante F, Roos BO, Gagliardi L (2010) Inorg Chem 49:5216
68. Zhao Y, Truhlar DG (2010) Chem Phys Lett. doi:10.1016/j.cplett.2010.11.060